NINETEENTH EUROPEAN ROTORCRAFT FORUM

Paper No. B 8

Experimental Results of the European HELINOISE Aeroacoustic Rotor Test in the DNW

W. R. Splettstoesser
DLR, Braunschweig
Germany

G. Niesl
ECD, Ottobrunn
Germany

D. G. Papanikas
ALFAPI, Athens
Greece

F. Cenedese
AGUSTA, Milano
Italy

F. Nitti
CIRA, Capua
Italy

September 14 - 16, 1993

CERNOBBIO (Como), ITALY

ASSOCIAZIONE INDUSTRIE AEROSPAZIALI
ASSOCIAZIONE ITALIANA DI AERONAUTICA ED ASTRONAUTICA

Experimental Results of the European HELINOISE Aeroacoustic Rotor Test in the DNW

W. R. Splettstoesser
DLR, Braunschweig
Germany

G. Niesl
ECD, Ottobrunn
Germay

F. Cenedese
AGUSTA, Milano
Italy

F. Nitti
CIRA, Capua
Italy

D. G. Papanikas
ALFAPI, Athens
Greece

ABSTRACT

In a major cooperative research program between 8 European partners, a 40%-geometrically and dynamically scaled and highly instrumented model of the ECD (formerly MBB) BO 105 helicopter main rotor was tested in the open jet anechoic test section of the German-Dutch Wind Tunnel, DNW, in the Netherlands. A comprehensive set of simultaneous acoustic and aerodynamic blade surface pressure data as well as blade dynamic and performance data were measured for the standard rotor with rectangular blade tips. The primary objective of this experimental study was to generate an extensive airload and acoustic data base and to examine the relation between the blade pressure characteristics and the acoustic radiation. Initial quantitative information on blade-tip vortex trajectories and blade positions during blade-vortex interactions was obtained. The blade pressure instrumentation, the experimental equipment used, the test procedures applied, and the scope of the test matrix conducted are briefly explained. Typical test results are presented in this report verifying the expected high data quality and consistency. The data is expected to improve the understanding of rotor aeroacoustics and to further the validation of various aerodynamic and acoustic codes developed or improved by the partners of this joint European venture.

INTRODUCTION

Within the European helicopter aeroacoustic research community it had long been recognized that rotor noise has become an important design parameter for the next generation of rotorcraft. This requires more refined and much more precise noise prediction tools than current aeroacoustic prediction methodology can provide (Ref. 1). The general objectives of this research program initiated and partly sponsored by the Commission of the European Communities (CEC) were to improve the physical understanding of rotor aerodynamics, acoustics, and dynamics and to further the development of numerical rotor simulation and design capabilities for future less noisy rotor systems. Detailed information on both the radiated sound field and the characteristics of the unsteady blade surface pressures together with well documented aeroelastic blade behavior and rotor operational conditions are crucial in improving and validating the aerodynamic and acoustic codes for the prediction of rotor noise. However, within the European helicopter noise research community such essential data was not available to the extent necessary.

Just after completion of the German-Dutch Wind Tunnel, DNW in 1982, a 1/7-scale AH-1/OLS model rotor experiment was jointly performed by AFFD and DLR under a Memorandum of Understanding between the United States and Germany. This rotor aeroacoustic demonstration test provided simultaneous acoustic and blade pressure results of 'benchmark' quality, however of limited quantity due to the small number of blade pressure sensors available (Refs. 2, 3, 4). In the mid-eighties inspired by the high quality of the AH-1/OLS model data a cooperative test of AFDD and Boeing Helicopter Co. on a 1/5-scale Boeing 360 model rotor was executed in the DNW to yield simultaneous information on acoustic and blade loading characteristics covering a rather complete test matrix (Refs. 5, 6). In 1988/89 DLR performed a main rotor/tail rotor aerodynamic interference noise study in the DNW on a 1/2.5-scale BO 105 rotor system featuring a pressure instrumented tail rotor with a limited number of pressure sensors. For a number of test conditions sychronous acoustic and blade pressure fields for the tail rotor in isolation and in combination with the main rotor were obtained (Ref. 7). In a major cooperative program between AFDD, NASA, UTRC, and Sikorsky Aircraft Division an extensive high quality airload and acoustic data base was established for the 1/5.7-scale current technology (swept tip) Sikorsky main rotor operated in the DNW (Refs. 8, 9, 10). Furthermore, over the past few years, a number of model rotor studies mainly focused on rotor impulsive noise (Refs. 11, 12) and its reduction e.g. by HHC (Refs. 13, 14) without blade pressure measurements were conducted by DLR with different partners like NASA LaRC, ECD, and ECF. In most cases, to a great

Presented at the 19th European Rotorcraft Forum,
Cernobbio, Italy, September 14 - 16, 1993

part due to the excellent flow quality and anechoic properties of the DNW, high quality aerodynamic and/or acoustic data were obtained. However, access to complete sets of simultaneous blade pressure and acoustic data necessary for the validation of aeroacoustic prediction codes was not available for the European rotor aeroacoustic research community.

To resolve this deficiency in Europe and following a major aeroacoustics research initiative by the CEC an extensive experimental program was launched under the acronym HELINOISE employing a geometrically and dynamically scaled and highly instrumented main rotor model of the BO 105 helicopter to be placed in a high quality aeroacoustic wind tunnel. The primary objective of the corresponding experimental effort was the generation of an extensive blade airload and acoustic data base and the examiniation of the relation between the blade pressure characteristics and the acoustic radiation. The secondary objective was the acquisition of detailed quantitative information on blade-tip vortex trajectories and related blade positions during blade-vortex interactions and the demonstration of the feasibility of optical measurements of blade deflections and the angle of incidence at the blade-tip. In order to meet the test objectives, one of the four rotor blades was extensively equipped with absolute-pressure sensors of the piezoresistive type to guarantee high spatial resolution of the blade pressure field. In addition, this blade and the remaining other blades were equipped with numerous strain gauges and a few temperature sensors.

Simultaneously to acquiring the unsteady blade surface pressure data, the acoustic radiation from the rotor was measured through a movable inflow microphone array placed at a distance of slightly more than one rotor radius below the rotor. The experimental set-up and specially developed data acquisition hard- and software was used to acquire both the acoustic radiation and the source related unsteady blade pressures within a test matrix covering a wide range of rotor conditions within - and even extending - the BO 105 helicopter flight envelope. The high quality aerodynamic and acoustic data obtained during the two-week tunnel entry are expected to improve the physical understanding of rotor aeroacoustics and to enhance the validation of various aerodynamic and acoustic codes developed or improved by different partners of this joint European effort.

The five organizations participating in the HELINOISE test program had specific responsibilities: AGUSTA and CIRA jointly provided funding for the wind tunnel and gave essential advice during the development of the test matrix. Both ECD and DLR were responsible for providing the pressure sensor instrumented rotor. Furthermore, DLR was responsible for the overall test coordination and for the complete test hard- and software. In particular DLR provided and operated the rotor test rig including its instrumentation and took the responsibility for the adaption of the instrumented rotor, for providing and operating the acquisition systems for blade aerodynamic, acoustic, and rotor performance data, and finally for on-line processing of the data for quick-look quality control. Post-processing of the digitized data for graphical documentation of the test results will be provided by ALFAPI supported by DLR.

The following sections briefly describe the experimental equipment used, the procedures applied, and the scope of the test matrix. Selected acoustic and aerodynamic results pertaining to blade-vortex interaction and high speed impulsive noise are presented, followed by initial results of the flow visualization effort. A complete documentation of the HELINOISE test is given in Ref. 15.

EXPERIMENTAL EQUIPMENT AND PROCEDURES

Wind Tunnel

The test was conducted in the open test section of the German-Dutch Wind Tunnel (DNW) located in the North East Polder, The Netherlands, which is known as one of the best aeroacoustic test facilities in existence. The DNW is a subsonic, atmospheric, closed circuit wind tunnel with three interchangeable, closed test section configurations and one open configuration. The open jet configuration used for this aeroacoustic test, employs an 8 x 6 m contraction section and a 19 m-long test section, surrounded by a large anechoic hall of about 30 000 m^3 lined with absorptive acoustic wedges (cut-off frequency of 80 Hz). The tunnel has low background noise and excellent fluid dynamic qualities, fully described in Refs. 16, 17.

Model Rotor Test Apparatus

MWM Test Stand and Support

The modular wind-tunnel model (MWM) rotor test stand (Ref. 18) was employed to drive the instrumented 'HELINOISE' model rotor. The test setup together with the inflow microphone traverse is shown installed in the DNW open test section in Figure 1. A diagram of the test apparatus with some important dimensions appears in Figure 2. Compared to the earlier DLR ROTEST rig the MWM features increased power capacity and a more compact design allowing more extended downstream acoustic measurements with the inflow microphone traverse. The remaining features were identical with the ROTEST specifications documented in Ref 19. Some details of the MWM are given in Table 1. The test stand consisted of three major subsystems: the hydraulic rotor drive system (130 kW), the rotor balance system using

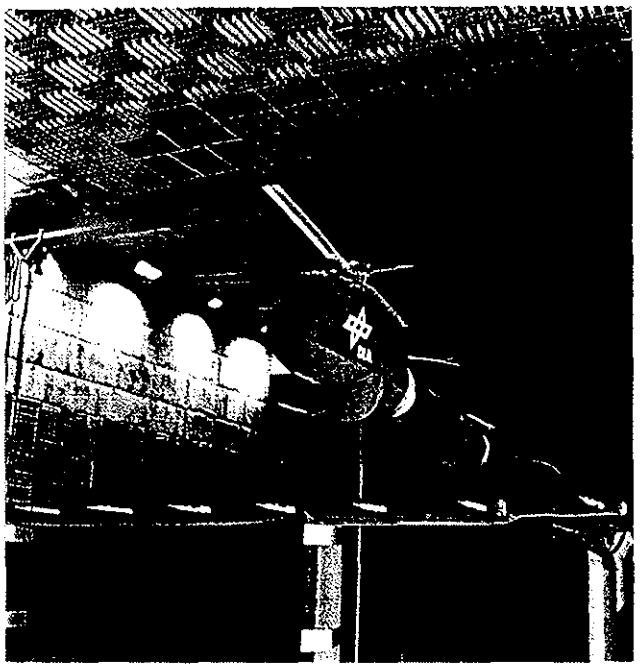

Figure 1 Model rotor test setup and inflow microphone array installed in the DNW open test section

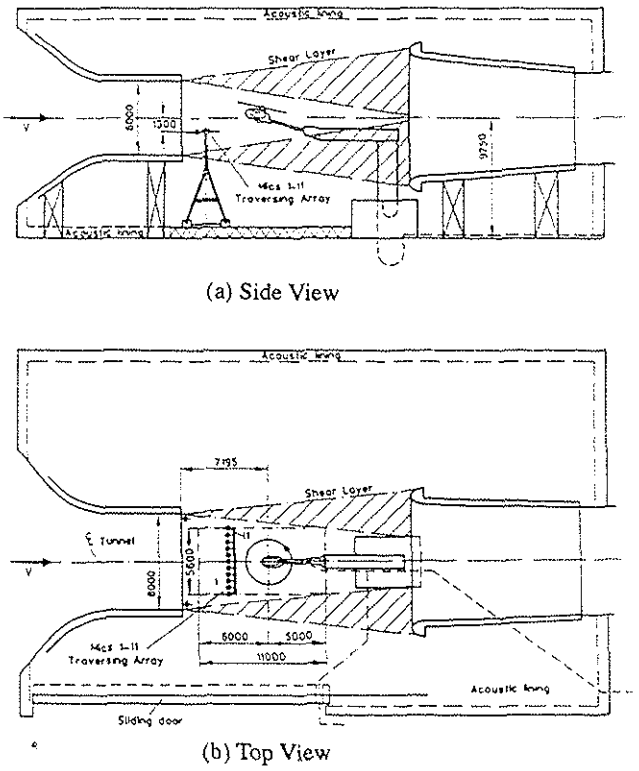

Figure 2 Schematic sketch of the test setup (dimensions mm).

separate measuring elements for static and dynamic load components, and the rotor control system comprising the swashplate and three computer-controlled electrodynamic actuators providing collective and cyclic pitch control. For more details refer to Ref. 18. The test rig was supported by the computer-controlled, hydraulically actuated model sting support mechanism of the DNW. It was housed within an acoustically insulated fiberglass shell, which was designed to largely reduce the hydraulic drive noise of the nine-piston axial hydraulic motor (fundamental frequency about 350 Hz). More details on the test setup is communicated in Ref. 15.

Model Rotor

The rotor tested was a 40%-geometrically and dynamically scaled model of the 4-bladed, hingeless BO 105 main rotor of 4 m diameter and 0.121 m chord length (Fig. 3(a)). The rotor blade was formed of a NACA 23012 airfoil with the trailing edge modified to form a 5 mm-long tab to match the full-scale rotor. The blades had -8° of linear twist (distribution shown in Fig. 3(b)), a square tip, and a solidity of 0.077. The nominal rotor operational speed was 1040 rpm, giving an acoustic blade passage frequency (bpf) of about 70 Hz. The nominal hover tip Mach number was 0.641. The rotor blades were made of glass- and carbon-fiber reinforced plastic with essentially the same mass- and stiffness distributions as the full-scale rotor. More detailed information on the rotor characteristics is given in Table 1 and on blade dynamic properties in Ref. 15.

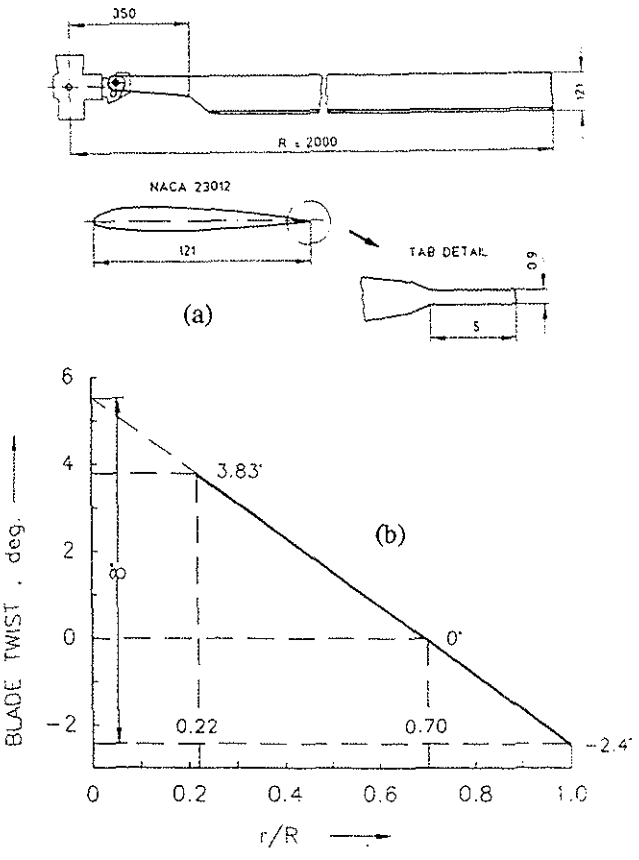

Figure 3 Blade geometry (a) and twist distribution (b)

Table 1 Details of the BO 105 model rotor and MWM test stand.

MAIN ROTOR:	
Rotor diameter, m	4.0
Blade chord, m	0.121
Blade airfoil section	NACA 23012
Number of blades	4
Blade twist (linear), deg	-8
Twist outboard of 0.44 m, deg	-6.23
Blade solidity	0.077
Blade tip speed, m/sec	218
Flapping frequency ratio (instrum. rotor @ 100% rpm)	1.126
Lagging frequency ratio (instrum. rotor @ 100% rpm)	0.78
Torsional frequency ratio (instrum. rotor @ 100% rmp)	4.05
Nominal rotational speed, rpm	1040
Nominal rotor thrust, N	3600
Lock number	8.0
Pre-coning angle, deg	2.5
DRIVE SYSTEM:	
Shaft power, kW	130
Rotor drive moment, N-m	1180 at 1050 rpm
BALANCE LOAD RANGE:	
Axial force, N	1000
Side force, N	2000
Thrust force, N	7000 static ±1500 dynamic
Rolling moment, N-m	700
Pitching moment, N-m	700
CONTROL SYSTEM:	
Blade setting angle range, deg	-4 to 14

Blade Instrumentation

One of the primary purposes of the experimental study was to measure the blade surface pressure distribution (aerodynamic blade loading) during rotor operation. Consequently, one of the rotor blades was equipped with a total of 124 specially configured miniature absolute-pressure transducers of the piezoresistive type, mainly installed at three blade sections (r/R = 0.75, 0.87, 0.97) with up to 44 sensors each per cross section, as illustrated in Figure 4. This includes one sensor each installed at the leading edge and trailing edge. Additional sensors were placed close to the leading edge at 3% chord on the blade

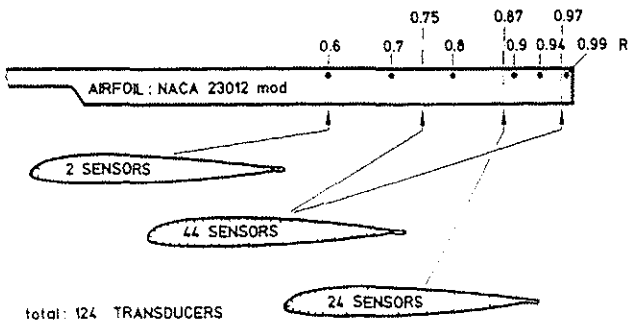

Figure 4 Pressure transducer distribution.

suction- and pressure-side along the blade span (r/R = 0.6, 0.7, 0.8, 0.9, 0.94, 0.99) The pressure transducers were of the Kulite LQ-32-064-25A type, with internal temperature compensation, specially designed for narrow installation to allow high spatial resolution of the blade pressure field. The transducers were submerged in the blade surface layer being in contact with the surface pressure field via small dimension, very short tubes (0.5 mm inner diameter, 0.6 mm length), such that the sensors effective measuring area corresponded to a circle of 0.5 mm diameter. Thus the essential high spatial resolution of the pressure field was ensured. Dynamic frequency response calibration was performed of each transducer prior to and after installation. Also, prior to installation the transducer response to a local white noise source was compared to the simultaneous output of a reference microphone (similar procedure as reported in Ref. 8). The frequency response of the installed transducers was obtained in a similar way, however, by application of a frequency sweep method up to 10 kHz. The typical response was flat within 1 dB up to 7 kHz with a resonance occurring beyond 10 kHz. Due to installation requirements the three trailing edge sensors had a lower resonance frequency.

The steady-state pressure calibration was conducted before and repeatedly during the DNW entry by placing the installed blade in a pressure sealed tube and measuring the output of all transducers simultaneously at different pressure levels (typically ambient and some pressure values below ambient). Steady-state calibration accuracy is estimated to be within 0.07 kPa.

The pressure instrumented blade (blade 1) was also equipped with 32 strain gauges. Blades 2, 3, and 4 contained seven strain gauges each and blade 2 three temperature sensors in addition (for pressure sensor thermal compensation purposes). Flapwise, edgewise, and/or torsional strains were measured at up to 16 radial stations between r/R = 0.14 and 0.83. Static calibrations were applied prior to the test. Calculated blade tip deflections resulting from the experimental strains are to be correlated later to optically measured tip deflections to verify the aeroelastic formulation in some partners' rotor simulation codes.

Acoustic Instrumentation

The acoustic instrumentation consisted of a linear inflow microphone array mounted on a ground based traverse system with a maximum range of 11 m in flow direction (Figs. 1, 2). The microphone array was shaped like a horizontal wing with its span normal to the flow and covered with open-cell foam to reduce reflections. Eleven microphones were arranged symmetrically with respect to the tunnel centerline and equally spaced 0.54 m apart. Two reference microphones were mounted on either side of the fuselage. The array vertical position was usually 2.3 m

(1.15 R) below the rotor hub, a distance just sufficient to allow farfield measurements of BVI impulsive noise (frequency content above 500 Hz, Ref. 11). The microphones were 1/2-inch pressure-type condenser microphones equipped with „bullet" nose cones. The microphone holders employed a „soft" vibration-isolation mounting. The traverse mechanism was powered by a variable-speed dc electric motor. Control and position (referenced to the rotor hub) was established with a servo position controller. Position accuracy was about 2 mm. Standard microphone calibration procedures were applied.

Data Acquisition Instrumentation

A scheme of the complete data acquisition system necessary to acquire simultaneous sets of blade pressure and acoustic data complemented by the related rotor performance and wind tunnel data collected in a common data base is diagrammed in Figure 5. The individual acquisition systems of DNW and DLR were all computer controlled and linked together via ETHERNET (ensuring easy data transfer) except the blade pressure measuring system which was linked indirectly via RS 232 to the rotor performance acquisition system. Synchronization between the systems was established by blade position reference signals (1/rev, 1024/rev, 2048/rev) supplied by a rotor azimuth angle encoder.

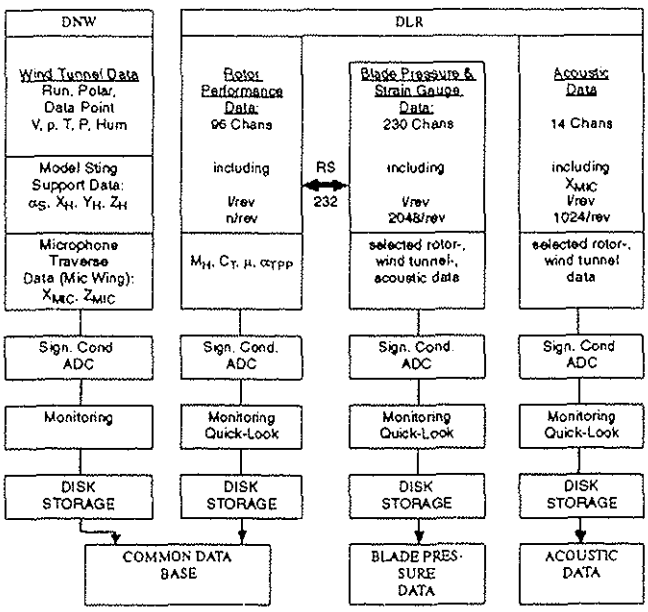

Figure 5 Schematic diagram of the HELINOISE data acquisition systems

After proper signal conditioning and antialiazing filtering the measuring signals were digitized for a number of revolutions (between 30 and 60) and stored on disk. The acoustic data together with synchronization signals were additionally recorded on a 14-track analog tape recorder for later analysis at higher resolution. 32 revolutions of rotor control, performance, and dynamic data (a total of 96 channels) were conditionally sampled at a rate of about 500 Hz and averaged in the time and frequency domain. The data base comprises steady-state and dynamic results (amplitude and phase) up to the 8th rotor harmonic.

Acoustic Data Acquisition and Analysis

A very time-efficient and sufficiently exact method was chosen to acquire the acoustic data in a large plane below the rotor. Termed „on-the-fly" data acquisition technique, the inflow microphone array was moved slowly (45 mm/s) and continuously over the measuring range of typically 4 to 5 R. The microphone signals were recorded together with the streamwise microphone position and the synchronizing signals on analog tape. For online analysis and quality control purposes the acoustic data were acquired every half meter in streamwise direction providing typically 200 acoustic measurement points for each rotor condition. At each pre-selected streamwise position the acoustic data acquisition system (Ref. 15) was started and all microphone signals (11 array microphones, 2 fuselage microphones) were conditionally sampled at a rate of 1024/rev over a period of 30 rotor revolutions (1.7 seconds), giving a useful frequency range of 9 kHz. The data shown here were generated offline at twice the online sample rate. The maximum angular displacement of the microphone array during the 1.7-second data acquisition period was 1.9° and it was verified (by comparison with instantaneous data, sample see Fig. 11) that the ensemble averaged acoustic data were not noticeably affected. The travel time (about 12 seconds) between the pre-selected acquisition locations was used to transmit the digitized data to the host computer for subsequent analysis, display, and plotting. Ensemble averaged sound pressure time histories as well as averaged narrow band power spectra (by FFT) were calculated. The data were further evaluated in terms of bandpass summary levels comprising low-frequency levels calculated from the 2nd to the 10th bpf harmonic (an approximate measure for thickness and high speed noise) and mid-frequency levels computed from the 6th to the 40th bpf harmonic (a representative measure for BVI impulsive noise). Finally, the results were presented in terms of isobar contour plots illustrating the noise radiation field of interest below the rotor.

Blade Pressure Data Acquisition and Analysis

The output signals of the 124 pressure transducers installed in one blade were pre-amplified by miniaturized amplifiers in the rotating frame (gain factor 125), transmitted via a 256-channel slipring system to the fixed frame, and simultaneously sampled at a rate of 2048/rev providing a useful frequency content up to 18 kHz. Raw data of 60 rotor revolutions were acquired and stored in the transputer memories for subsequent calculation of

ensemble averaged time histories and narrow band power spectra via FFT. It appears worthwhile to mention that for this test a multichannel (352) specially configured 'transputer based expandible data acquisition system (TEDAS)' was developed by DLR, which was composed of 44 'intelligent data acquisition modules (IDAMS)'. Each module consisted of a transputer (T800), 4 MByte RAM and eight 16-bit A/D-converters of 44 kHz sample frequency. Because of the choice of Delta Sigma ADCs and application of digital filtering expensive analog filters were not required (Refs. 15, 20). Data pre-processing with TEDAS was very time-efficient since all transputer modules were working in parallel, so that shortly after the test the measurement results (pressure histories and distributions) were available for display and plotting. The raw data of 60 rotor revolutions, the averaged, and pre-processed data were finally stored on digital tape for later evaluation.

Data Quality Guarantee

The stability and steadiness of the test conditions as well as the consistency and repeatability of the measurement results were checked and verified, to ensure a high quality standard of the measured aerodynamic and acoustic data. The results are presented in a later section. Prior to starting the measurement program, reflection tests employing explosive charges placed in the rotor plane were performed to verify the anechoic test environment and to identify possible areas in the acoustic measurement plane that might be affected by acoustic shielding by the rotor drive fairing or the model support sting. Wind tunnel background noise measurements at different airspeeds were taken to ensure a proper signal-to-noise ratio. Detailed results of these efforts are presented in Ref. 15.

Matrix of Test Conditions

The test matrix represents a large number of simulated flight conditions comprising climb, level flight, and descent with flight path angles ranging from 12° climb up to 12° descent and flight velocities from zero (hover) up to 80 m/s covering the major part of the BO 105 flight envelope - even extending it in the high speed regime. Major emphasis was put on rotor conditions known to generate rotor impulsive noise, i.e. blade-vortex interaction (BVI) and high-speed impulsive (HSI) noise. To enforce HSI noise radiation the rotor tip speed was increased by 5% beyond the nominal RPM to realize an advancing blade-tip Mach number of more than 0.9.

Flow visualization using a laser light sheet (LLS) technique, was applied to obtain quantitative information on details of the blade-vortex interaction geometry like blade vortex missdistance and orientation and shape of sections of the tip vortex trajectories close to and during BVI. In addition, limited blade-tip deflection measurements by making use of a videographic technique were included.

TEST RESULTS

In the following sections typical test results pertaining to the acoustic, the aerodynamic blade pressure, and flow visualization measurements are presented.

Acoustic Results

BVI Impulsive Noise

Typical blade-vortex interaction impulsive noise characteristics for a low speed 6°-descent condition (ICAO noise certification landing approach) are shown in Figure 6. The mid-frequency level contour plot illustrates the sound field underneath the rotor at a distance of z/R = 1.15, clearly indicating two high intensity noise radiation lobes of, respectively, advancing side BVI and retreating side BVI. The related sound pressure time histories reveal the typical positive pressure spikes of advancing side BVI as well as the negative pressure spikes of retreating side BVI. The corresponding power spectra illustrate the impulsive nature of BVI noise mainly distributed in the mid-frequency range approximately between the 6th and the 40th blade passage frequency harmonic.

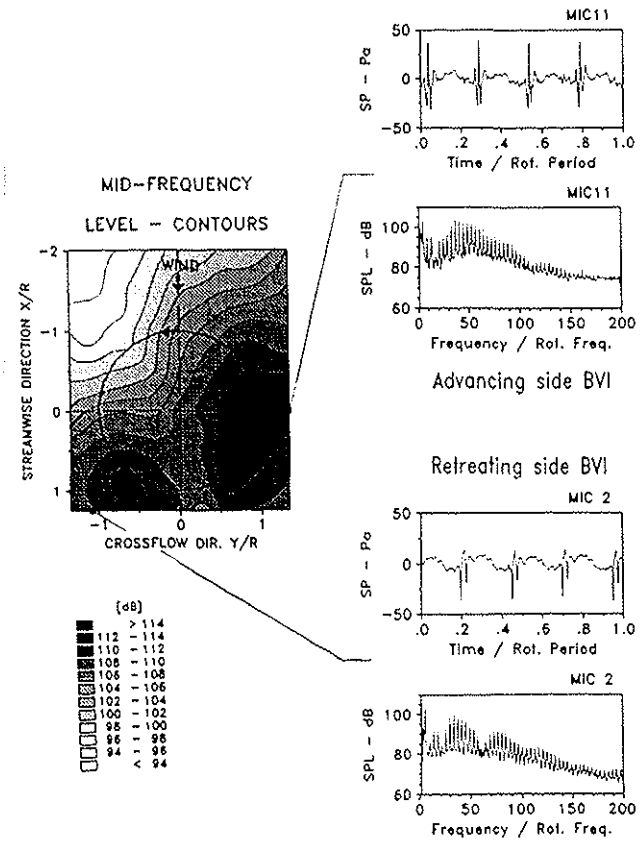

Figure 6 Typical BVI impulsive noise characteristics for a 6°-descent condition (μ = 0.149, α_s = 5.3°, C_T = 0.0045, M_H = 0.644).

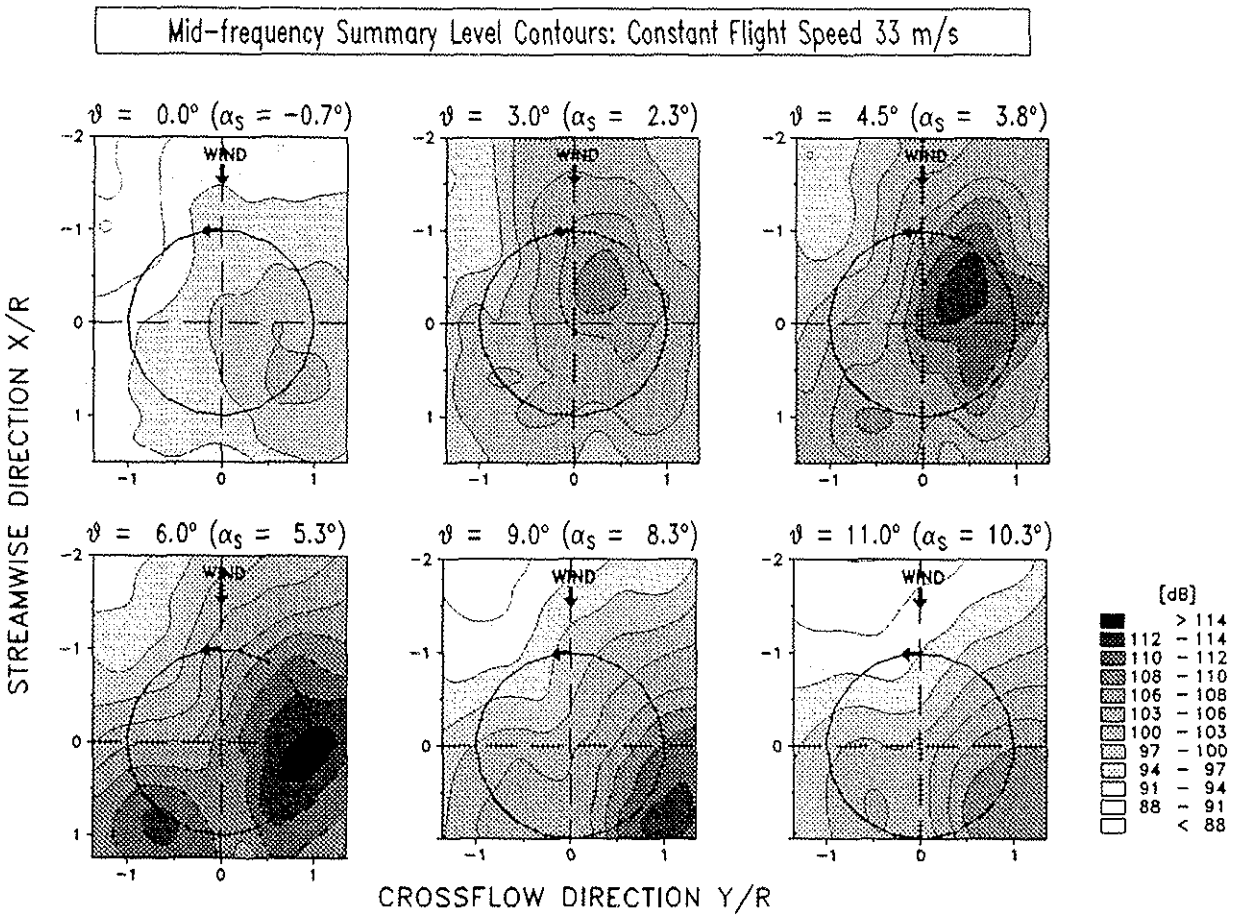

Figure 7 Effect of flight path angle ϑ (or shaft angle α_s) on BVI noise radiation ($\mu = 0.150$, α_s = var., $C_T = 0.0044$, $M_H = 0.641$).

BVI noise generation and radiation are strongly dependent on flight condition. The influence of flight path angle (or of tip-path-plane inclination) at constant airspeed of 33 m/s is illustrated by the series of mid-frequency level contour plots in Figure 7 ranging from level flight to 11°-descent. Strong changes in BVI noise directivity and intensity are seen. Maximum intensities have been observed between 5°- and 8°-descent.

Similar changes of the BVI noise directivity and intensity were measured when at fixed glide slope angle the flight velocity (or advance ratio) was varied. Even more intensive BVI noise radiation was found to occur for certain combinations of descent angle and airspeed, for which the trailing blade-tip vortex system is estimated to be close to the rotor plane. Thus it appears that for this rigid rotor depending on the descent angle strong BVI noise is generated over the complete speed range tested (Ref. 15).

High-Speed Impulsive Noise

At increasing forward speed and/or blade-tip speed both resulting in growing advancing blade-tip Mach number, thickness noise and beginning non-linear compressibility effects of high-speed impulsive noise become sinificant contributors to the total rotor noise radiation.

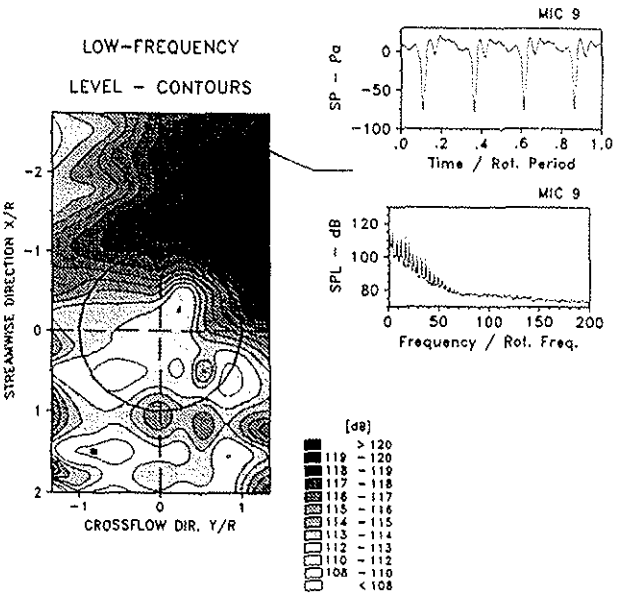

Figure 8 Typical high speed impulsive noise characteristics ($\mu = 0.347$, $\alpha_s = -13°$, $C_T = 0.0045$, $M_H = 0.640$).

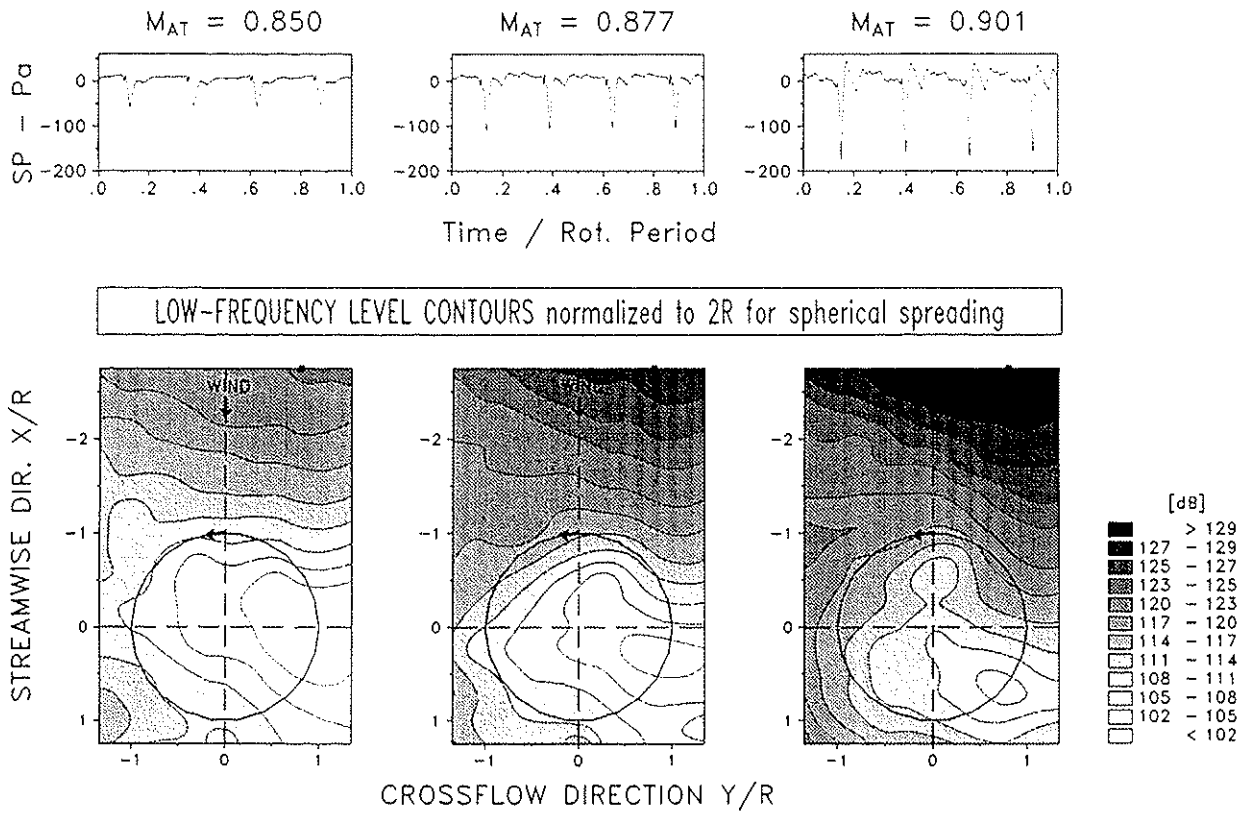

Figure 9 Effect of advancing blade-tip Mach number on high speed noise radiation (μ = 0.26, 0.30, 0.35, and α_s = -3.3°, -5.8°, -8.7°, respectively at C_T = 0.0044, M_H = 0.673; low frequency summary levels normalized to 2R for sperical spreading assuming source at blade tip and 90° azimuth angle).

An example of the typical negative pressure pulses of high-speed impulsive noise is shown in Figure 8 for an 80 m/s-level flight at an upstream microphone position (x/R = 2.5) on the advancing side. Such pressure pulses do not exist at the downstream (retreating side) location. The low-frequency level contour plot (here comprising the 2nd to the 10th bpf harmonic) illustrate the typical high speed noise directivity pattern directed upstream and toward the advancing side (with highest levels in the rotor plane, Ref. 2). The corresponding power spectrum shows increased levels of the bpf harmonics in the lower frequency range, typical for the onset of high-speed impulsive noise.

The dominant effect of the advancing blade-tip Mach number on the development of the high-speed impulsive noise waveform and directivity pattern is illustrated in Figure 9, where low-frequency contour plots and averaged sound pressure histories at an upstream, advancing-side, observer positions (x/R = 2.9, y/R = 0.8) are compared for three flight conditions (3°-descent) with increasing forward speed of 60, 70, 80 m/s. In order to enhance possible shock delocalization (known to occur around M_{AT} = 0.9) the rotor tip speed was increased by 5% beyond the nominal value giving corresponding advancing blade-tip Mach numbers of 0.850, 0.877, 0.901.

Steadiness and Repeatability of the Acoustic Data

Both steady wind tunnel flow and stable rotor operation are a prerequisite for the acquisition of high quality aeroacoustic data. During the test period a number of check points with identical test conditions were acquired to ensure consistency and repeatability of the test data. Instantaneous and averaged sound pressure time histories for a typical low speed 6°-descent condition with strong BVI are compared in Figures 10(a) and (b), illustrating the excellent steadiness and stability of the test conditions and also justifying the acoustic „on-the-fly" data acquisition technique applied. Comparison of the averaged acoustic signatures acquired on different days (Figs. 10(b) and (c)), demonstrates the superb repeatability for this flight case involving substantial blade vortex interactions (as seen in the related blade surface pressure data). Blade-to-blade variations are small indicating that the blades were well in track. Another even more convincing repeatability check is presented in Figure 11, where the on-line generated mid-frequency summary level contours representing the sound field below the rotor are compared for the same 6°-descent flight conditions, allowing detailed comparison of the BVI noise directivity and intensity. Marginal directivity changes on the retreating side are thought to be caused by adjustment of the rotor rpm to maintian constant tip Mach number, thus marginally affecting blade dynamics and the interaction geometry of the very strong retreating side BVI (see Fig. 15).

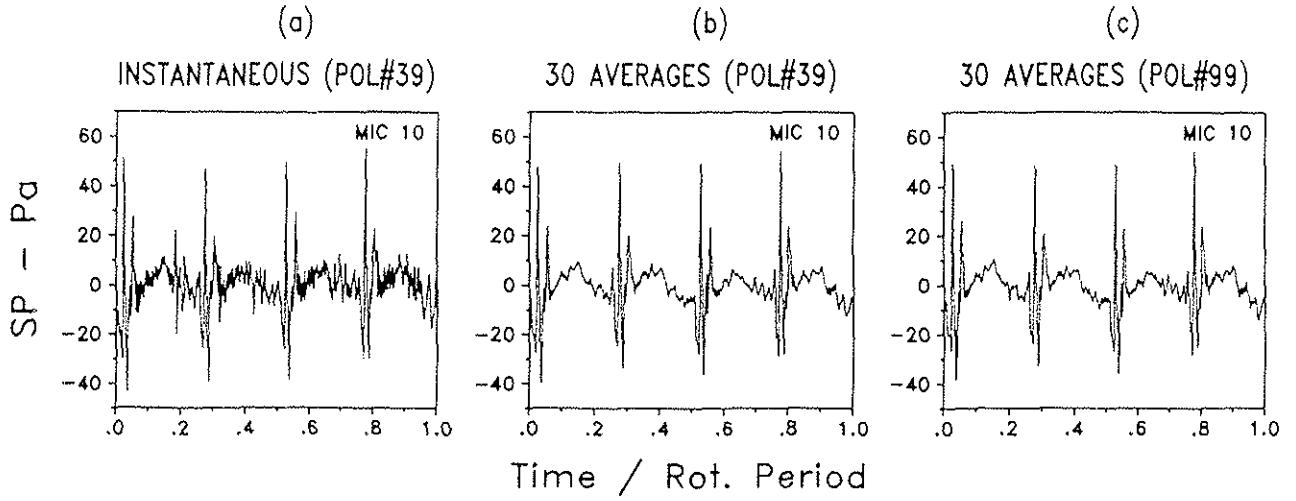

Figure 10 Steadiness and repeatability of local acoustic measurements ($\mu = 0.149$, $\alpha_s = 5.3°$, $C_T = 0.0045$, $M_H = 0.644$).

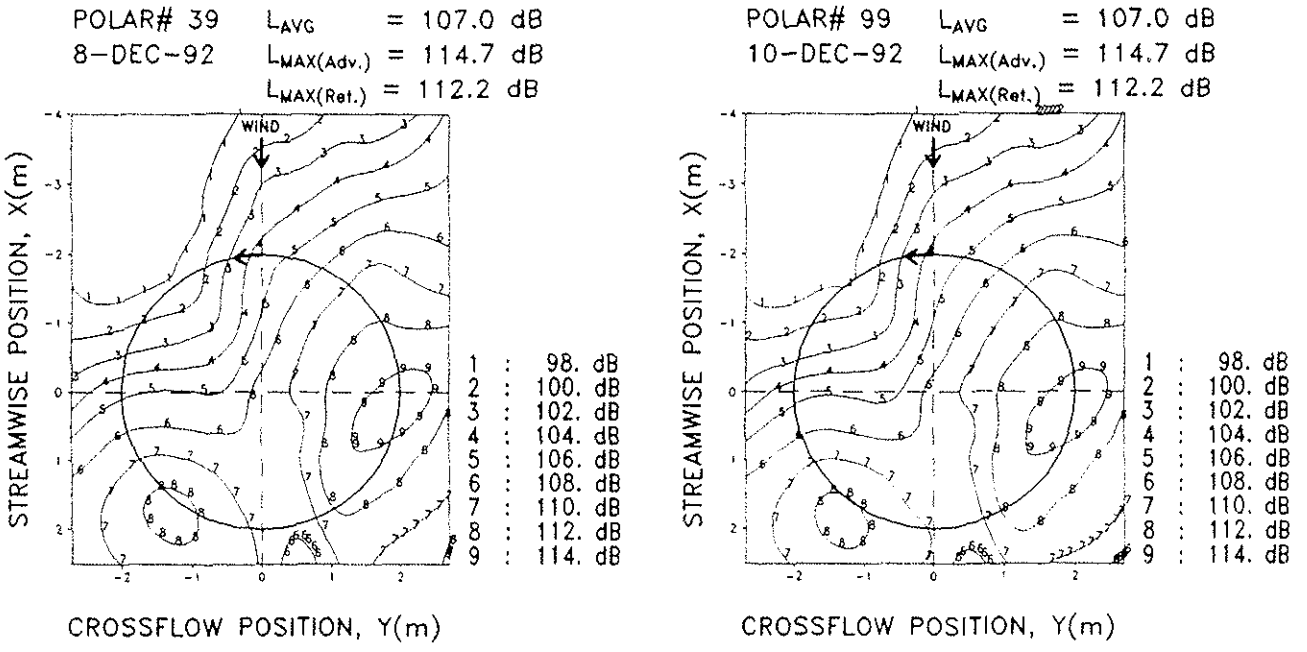

Figure 11 Repeatability of noise directivity and intensity measurements. (Mid-frequency level contours for check points at $\mu = 0.149$, $\alpha_s = 5.3°$, $C_T = 0.0045$, $M_H = 0.644$).

Aerodynamic Results

Unsteady Blade Surface Pressures

Samples of the blade surface pressure data are presented either as time histories for specific sensors or in form of chordwise distributions for specified radial and azimuthal positions. Figures 12(a) and (b) show time histories of the averaged pressure coefficient (60 averages). Pressures from ten selected transducers on the upper surface at r/R = 0.87 for a 6°-descent condition at $\mu = 0.150$ (Fig. 12(a)) show impulsive pressure fluctuations due to BVI on the advancing side ($15° < \psi < 90°$) and on the retreating side ($270° < \psi < 330°$), most significant close to the blade's leading edge. Similar fluctuations, however, with opposite polarity are measured on the lower surface. Pressure histories from ten transducers on the lower surface at r/R = 0.87 for a high speed level flight at $\mu = 0.347$ (Fig. 12(b)) show supersonic pockets near the leading edge during passage of the blade through the second quadrant ($90° < \psi < 140°$). The sharp azimuthal (or time) gradients confirm the requirement for high resolution pressure measurements with a useful frequency range of at least 5 to 8 kHz.

Chordwise Pressure Distributions

Figure 13 shows chordwise distributions of the blade pressure coefficient, C_p (normalized using the local relative dynamic pressure), for a high speed level flight at $\mu =$

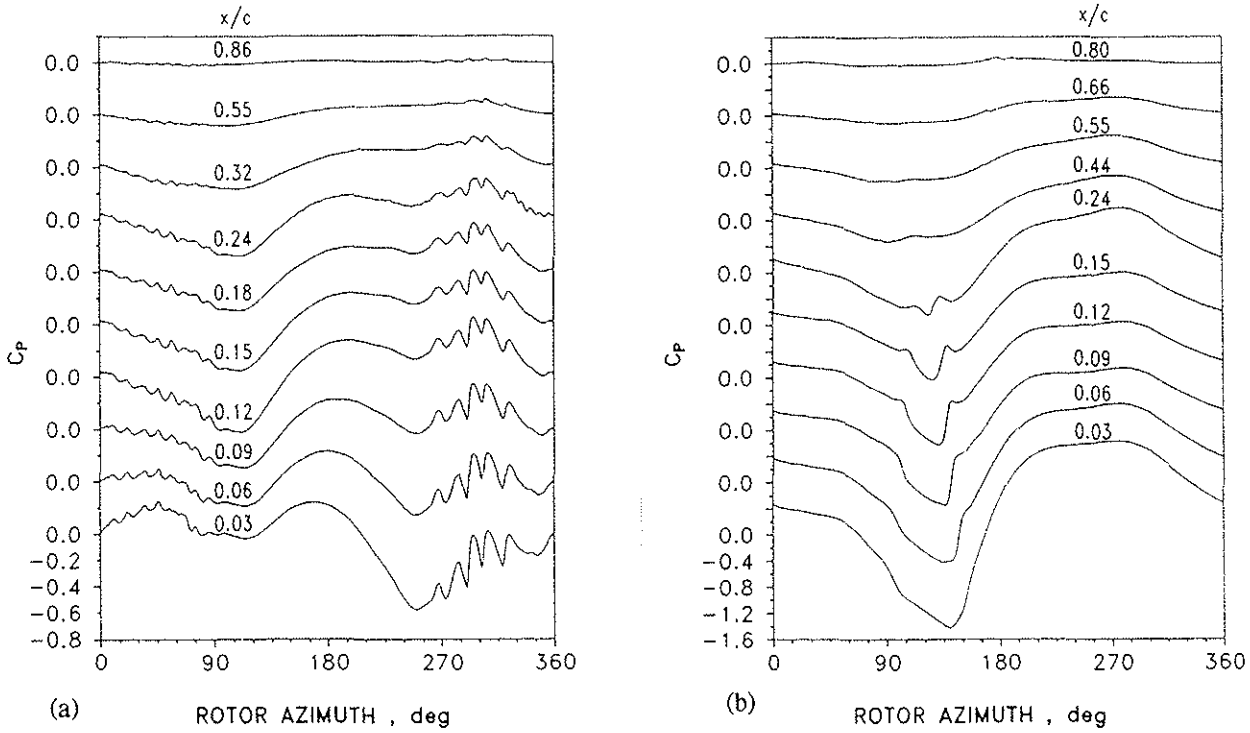

Figure 12 Blade pressure time histories at r/R = 0.87. (a) Upper surface: 6°-descent at μ = 0.149, α_s = 5.3°, C_T = 0.0045, M_H = 0.644, (b) Lower surface: level flight at μ = 0.347, α_s = -13°, C_T = 0.0045, M_H = 0.640, (AC pressure part only).

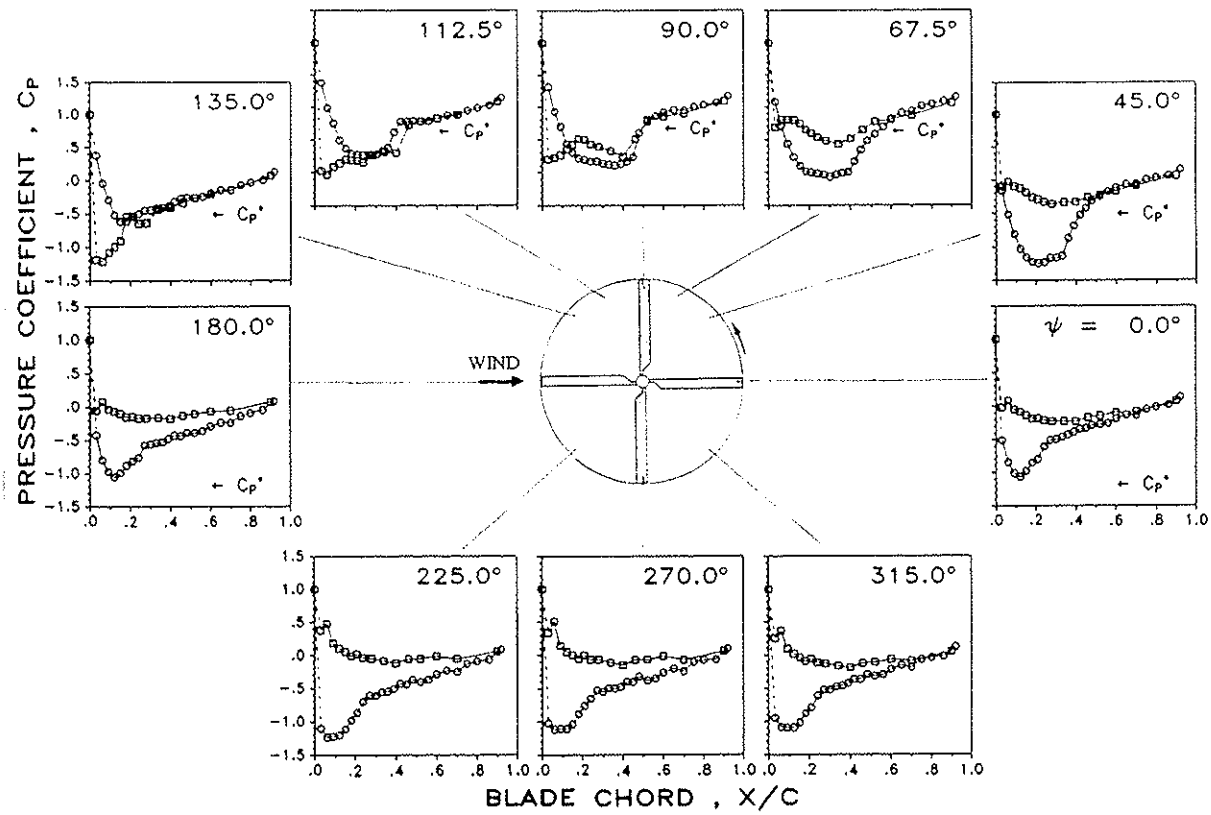

Figure 13 Chordwise blade pressure distributions for high speed level flight at μ = 0.347 (other conditions as for Fig. 12 b).

0.347, for ten selected azimuthal positions at r/R = 0.97. At Ψ = 45° the blade load is positive and the upper surface flow is supersonic with formation of a shock at the end of this region. The critical C_p^* values for the approximate sonic pressure are indicated by small arrows. At ψ = 90° and more clearly at 112.5° both upper and lower side indicate supersonic flow and shock formation. At ψ = 112.5° and 135° the blade load is negative (upper surface pressures larger than lower surface pressures). In the third and fourth quadrant, the load is again positive (with subsonic flow on the upper side).

force per unit area normal to the blade chord, normalized by the local chord (here constant) and relative dynamic pressure. Impulsive load fluctuations due to BVI on the advancing and retreating side are quite obvious. A very close BVI is seen at r/R = 0.97 near 300° azimuth. Further results pertaining to BVI impulsive loads are extensively discussed in Ref. 21.

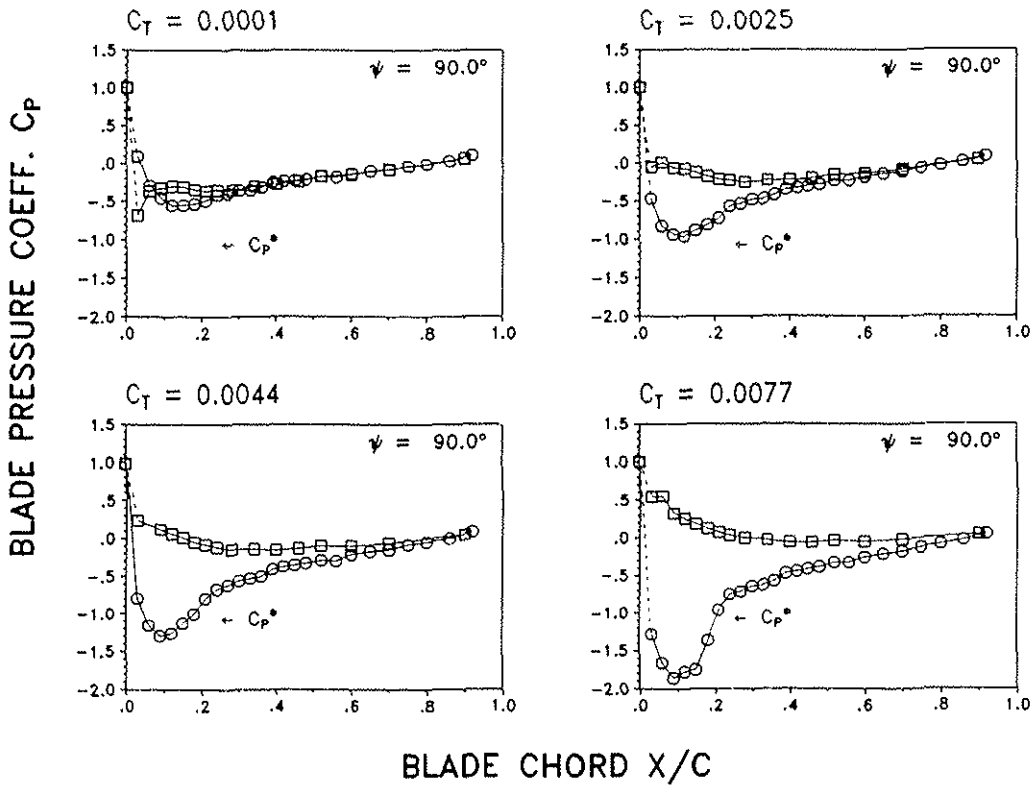

Figure 14 Chordwise blade pressure distributions at r/R = 0.97 for hover cases with different thrust settings (M_H = 0.64, α_s = 0°).

Chordwise pressure distributions (r/R = 0.97) for hover condition (M_H = 0.64) at four different thrust settings ranging from C_T = 0.0001 to 0.0077 are presented in Figure 14. For the highest thrust coefficient the C_p values are quite high and an extended supersonic flow region on the upper surface is seen. The pressure data are generally smooth and very consistent. It should be noted that all pressure data shown are as measured data without any smoothing or corrections.

Blade Airloads

Local blade airloads were calculated by integration of the measured blade pressures at each radial station. Normal force (C_N) time histories for a 6°-descent condition with strong BVI are shown in Figure 15. C_N is defined as the

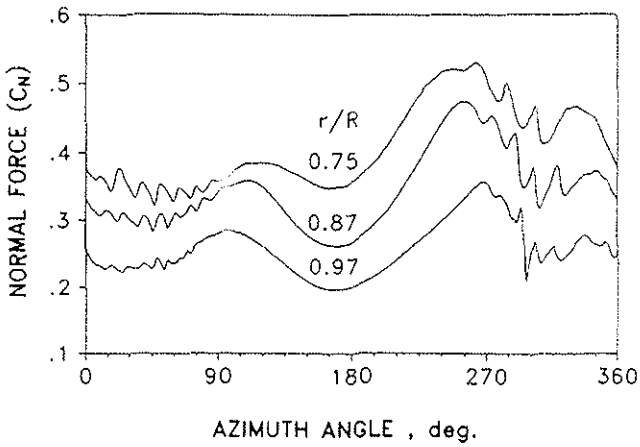

Figure 15 Normal force time histories for a 6°-descent condition (rotor condition as for Fig. 12 a).

Steadiness and Repeatability

Again, several check points with identical test conditions (6°-descent and high speed level flight) were acquired at different times. Figures 16(a), (b), (c) show a comparison of instantaneous and averaged (60 avgs.) blade pressure (C_p) histories for an upper surface sensor near the leading edge (x/c = 0.03; r/R = 0.87). Test condition stability and steadiness is illustrated by comparing the instantaneous (Fig. 16(a)) and the averaged (Fig. 16(b)) waveforms, while the high degree of repeatability is demonstrated by comparison of the averaged waveforms of Fig. 16(b) and Fig. 16(c) for this delicate BVI test condition. Excellent repeatability is verified also for high speed level flight condition at $\mu = 0.35$, as is illustrated in Figure 17 where chordwise pressure distributions, indicating supersonic flow and shock formation (partly on both surfaces), for nominal identical test conditions are compared.

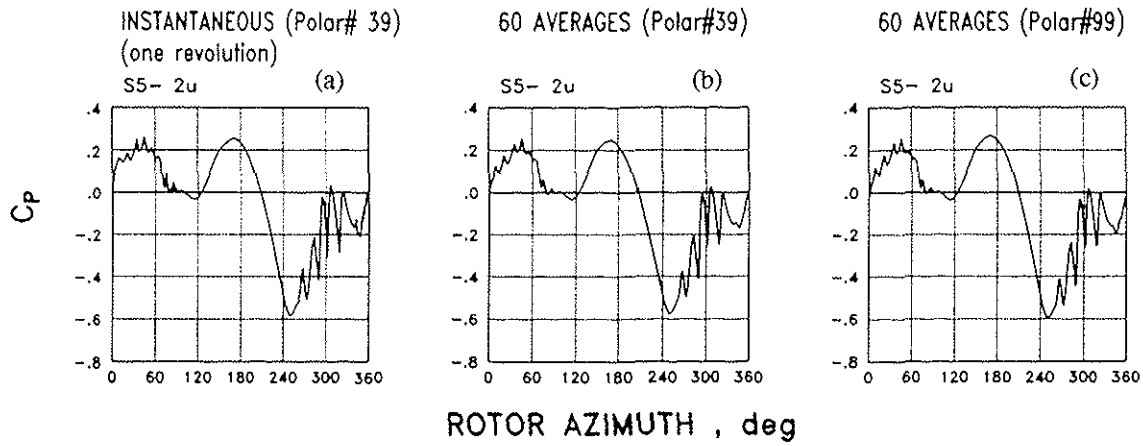

Figure 16 Steadiness and repeatability of local blade surface pressure measurements (AC part only, rotor condition of check points as for Fig. 12 a).

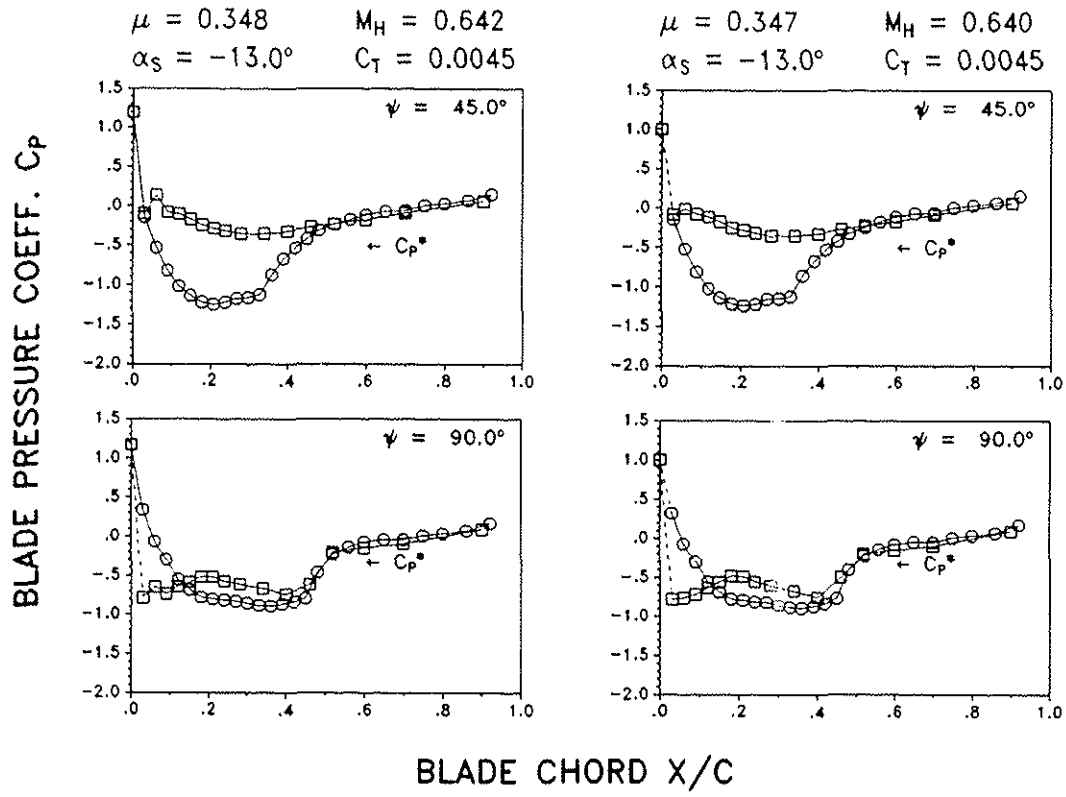

Figure 17 Repeatability of chordwise pressure distribution measurements (high speed level flight check points at $\mu = 0.35$).

Flow Visualization Results

Blade-Vortex Separation Distance

The laser light sheet (LLS) technique (Ref. 22) used for the flow visualization experiment provided initial quantitative results for the separation distance between blade-tip vortex and blade passing plane which represents a key parameter for the BVI phenomenon. By repeated application of the LLS technique a number of discrete vortex core positions for a fixed blade position was determined and used to reconstruct sections of the vortex trajectories being of greatest interest for advancing side BVI. Figures 18(a), (b) display both the top view (a) and frontal view (b) of a number of measured tip vortex trajectories for a typical BVI case (6°-descent at $\mu = 0.15$, $\alpha_s = 5.3°$). The data recording took place whenever the blade was at azimuth of 50°. In Figure 18(a) the measured results, indicated by crosses, are compared to calculated trajectories based on a simple flat wake model and indicate quite good agreement. The frontal view (Figure 18(b), looking downstream with the wind) shows the rotor blade and the measured sections of the vortex trajectories now projected into a vertical plane placed at an azimuth angle of 90°.

Due to the positive shaft angle all measured trajectories are located above the rotor plane. It should be noted that ΔZ represents the measured vertical distance of the vortex core to the blade path plane. The acoustically most important, nearly parallel and closest BVI occurs between 50° and 55° azimuth with vortex no. 6 which is approximately 450° old. Additional interactions are seen to occur with vortices no. 5 and no. 4, however, at larger azimuth and greater intersection angles and therefore acoustically less effective. The results for a level flight ($\alpha_s = -0.7°$) at otherwise identical test conditions is depicted in Figure 19. Most of the vortices in the first quadrant are now below the rotor plane. Vortex no. 6 (parallel to the blade leading edge) is far below and acoustically insignificant. Localized BVI due to large intersection angles is seen to occur with vortices no. 2 and no. 3, but acoustically less effective as well. These findings explain and illustrate the general observation that BVI noise is largely reduced at level flight (see Fig. 7). A table of the measured separation distance values is provided in the detailed test report of Ref. 15.

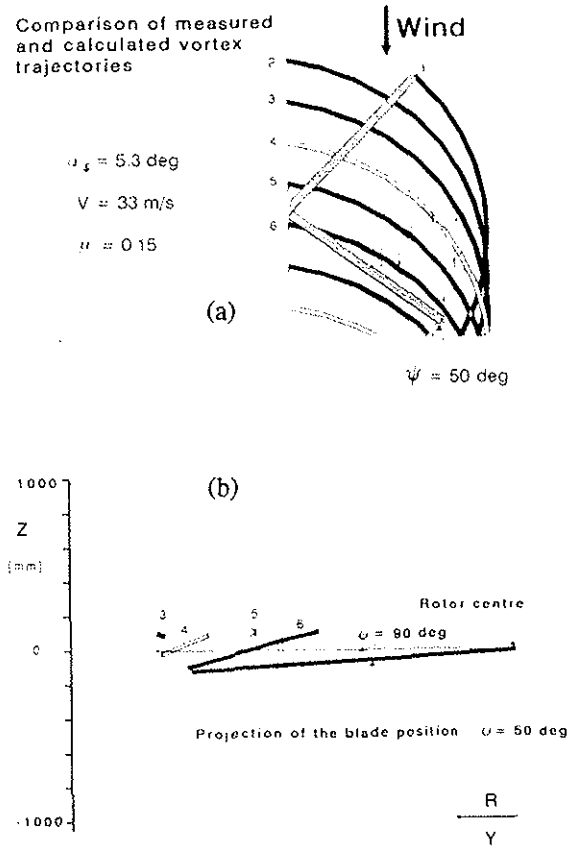

Figure 18 Measured vortex trajectory sections for a low speed descent condition, ($\mu = 0.15$, $\alpha_s = 5.3°$, $C_T = 0.0044$, $M_H = 0.641$), (a) plan view, (b) frontal view

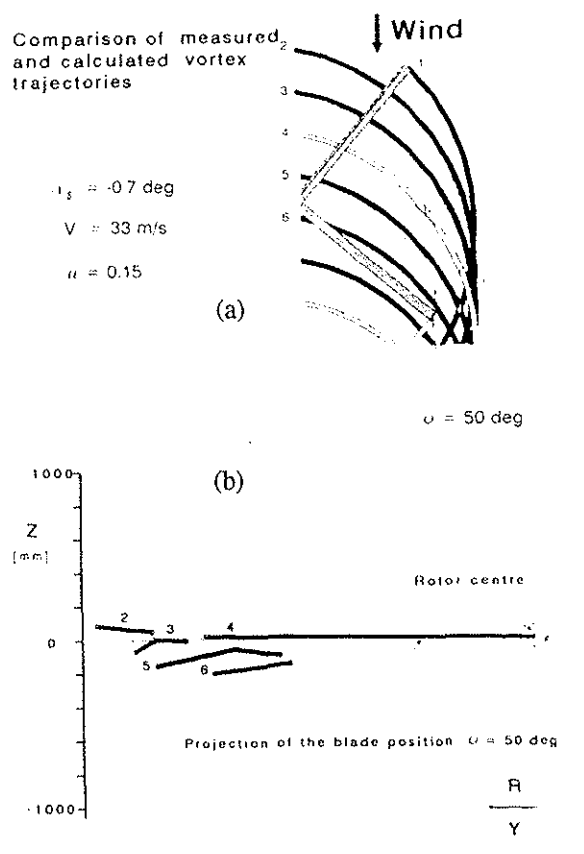

Figure 19 Measured vortex trajectory sections for a low speed level flight, ($\mu = 0.15$, $\alpha_s = -0.7°$, $C_T = 0.0044$, $M_H = 0.641$), (a) plan view, (b) frontal view

Blade Tip Deflections

Initial results from blade tip deflection measurements in flap, lag, and torsional directions using a videographic technique provided by DNW are reported in Refs. 15, 22. These data taken for fixed azimuth angles of 270° and 300° represent relative measurements for the variation of thrust from 2600 N to 3600 N at $\mu = 0.15$. The data are thought to be very useful for comparison with the calculated blade motions based on the conventional strain gauge measurements, but also for aeroelastic code validation purposes.

CONCLUDING REMARKS

Supported by the European Community and in close cooperation between research establishments (DLR and CIRA) and industry (ECD, AGUSTA, ALFAPI) from different European countries a very ambitious test was successfully completed. This was accomplished in a large part by jointly providing the expertise, funding, and manpower for the common research goal.

For an extensive matrix of test conditions the acoustic pressure field was measured by a traversing inflow microphone array consisting of 11 microphones. A total of 124 blade surface pressure transducers and 32 strain gauge sensors all installed in one blade were used to acquire the unsteady airloads and blade dynamic characteristics simultaneously with the acoustic pressure field. In addition, the laser light sheet flow visualization technique provided initial quantitative information on the blade-tip vortex trajectory geometry and blade-vortex separation distance, which represent key parameters for the BVI phenomenon. In summary, a very comprehensive aerodynamic and acoustic data base was simultaneously measured together with wind tunnel, rotor performance and blade dynamic data covering the complete flight envelope of the BO 105 main rotor.

This wealth of high quality aeroacoustic data, not available in Europe to this extent before, provides the basis to validate the computational methods, developed or improved by the theoretical research effort within the HELINOISE project (Ref. 23). Such basic and precompetitive prediction tools individually developed and jointly validated, are necessary prerequisites for the development of quieter advanced rotor systems.

ACKNOWLEDGEMENTS

In a test of such complexity, there are many people who deserve recognition for a job professionally and well done. The authors would like to offer their sincere thanks to their friends and colleagues of the following organizations:

DLR: Bernd Junker, Klaus-Juergen Schultz, Wolfgang Wagner, Heino Buchholz, Gunter Braun, Hans-Guenter Nolle, and their supporting technician team.

DNW Foundation: The professional test support team of its parent organizations DLR and NLR and with special recognition for providing the LLS flow visualization technique: Edzard Mercker and Kurt Pengel

REFERENCES

1. Lowson, M.V.: „Progress Towards Quieter Civil Helicopters", Paper No. 91-59, Proceedings, 17th European Rotorcraft Forum, Berlin, September 1991.

2. Splettstoesser, W.R., Schultz, K.-J., Schmitz, F.H., Boxwell, D.A.: „Model Rotor High Speed Impulsive Noise - Parametric Variations and Full-Scale Comparisons", American Helicopter Society 39th Annual National Forum, St. Louis, Missouri, May 1983.

3. Boxwell, D.A., Schmitz, F.H., Splettstoesser, W.R., Schultz, K.-J.: „Model Helicopter Rotor High-Speed Impulsive Noise: Measured Acoustics and Blade Pressures", NASA TM 85850, and US-AAVRADCOM TR-83-A-14, September 1983.

4. Splettstoesser, W.R., Schultz, K.-J., Boxwell, D.A., Schmitz, F.H.: „Helicopter Model Rotor Blade/Vortex-Interaction Impulsive Noise, Scalability and Parametric Variations", Proceedings 10th European Rotorcraft Forum, The Hague, August 1984 and NASA Techn. Mem. 86007, TM-84-A-7.

5. Dadone, L., Dawson, S., Boxwell, D.A., Ekquist, D.: „Model 360 Rotor Test at DNW- Review of Performance and Blade Airloads Data", American Helicopter Society 43rd Annual National Forum, St. Louis, Missouri, May 1987.

6. Zinner, R.A., Boxwell, D.A., Spencer, R.H.: „Review and Analysis of the DNW/Model 360 Rotor Acoustics Data Base", 15th European Rotorcraft Forum, Amsterdam, September 1989.

7. Schultz, K.-J., Splettstoesser, W.R.: „Model Tail Rotor Noise Study in the DNW - Measured Acoustics, Blade Pressures, Noise Predictions -", Paper No. 78, Proceedings, 18th European Rotorcraft Forum, Avignon, September 1992.

8. Yu, Y.H., Landgrebe, A.J., Liu, S.R., Lorber, P.F., Jordan, D.E., Pollack, M.J. Martin, R.M.: „Aerodynamic and Acoustic Test of a United Technologies Model Scale Rotor at DNW", Proceedings pp. 1233-1250, American Helicopter Society 46th Annual Forum, Washington DC, May 1990.

9. Liu, S.R., Marcolini, M.A.: „The Acoustic Results of the United Technologies' Scale Model Helicopter Rotor Tested at the DNW", American Helicopter Society 46th Annual Forum, Washington DC, May 1990.

10. Lorber, P.F.: „Aerodynamic Results of a Pressure-Instrumented Model Rotor Test at the DNW", American Helicopter Society 46th Annual Forum, Washington DC, May 1990.

11. Martin, R., Splettstoesser, W.R., Elliot, J., Schultz, K.-J.: „Advancing Side Directivity and Retreating Side Interactions of Model Rotor Blade Vortex Interaction Noise", NASA Techn. Paper 2784 and AVSCOM Technical Report 87-B-3-, 1988.

12. Splettstoesser, W.R., Schultz, K.-J., Martin, R.M.: „Rotor Blade-Vortex Interaction Impulsive Noise Source Localization", AIAA Journal, Vol. 28, No. 4 (1990), pp. 593-600.

13. Splettstoesser, W.R., Schultz, K.-J., Kube, R., Brooks, T.F., Booth, E.R., Niesl, G., Streby, O.: „BVI Impulse Noise Reduction by Higher Harmonic Pitch Control: Results of a Scaled Model Rotor Experiment in the DNW", Paper 91-61.1 Proceedings, 17th European Rotorcraft Forum, Berlin, September 1991.

14. Kube, R., Achache, M., Niesl, G. Splettstoesser, W.R.: „A Closed Loop Controller for BVI Impulsive Noise Reduction by Higher Harmonic Control", Proceedings, American Helicopter Society 48th Annual Forum, Washington DC, June, 1992.

15. Splettstoesser, W.R., Junker, B., Schultz, K.-J., Wagner, W., Weitemeier, W., Papanikas, D.G.: „The HELINOISE Aeroacoustic Rotor Test in the DNW", DLR-Mitteilungen 93-09, 1993.

16. Van Ditshuizen, J.C.A., Courage, G.D., Ross, R., Schultz, K.-J.: Acoustic Capabilities of the German-Dutch Wind Tunnel (DNW)", AIAA-83-0146, January 1983.

17. Boxwell, D.A., Schmitz, F.H., Splettstoesser, W.R., Schultz, K.-J., Lewy, S., Caplot, M.: „A Comparison of the Acoustic and Aerodynamic Measurements of a Model Rotor Tested in Two Anechoic Wind Tunnels", NASA TM-88364 and USAAVSCOM TM-86-A-6, 1986.

18. Stephan, M, Kloeppel, V., Langer, H.-J.: „A New Wind Tunnel Test Rig for Helicopter Testing", Paper No. 66, 14th European Rotorcraft Forum, September 1988.

19. Langer, H.-J. (SCITRAN, transl.): „DFVLR Rotorcraft - Construction and Engineering", NASA TM-77740, 1984.

20. Gelhaar, B., Junker, B., Wagner, W.: „DLR-Rotor Teststand Measures Unsteady Rotor Aerodynamic Data", Paper No. C 8, Proceedings, 19th European Rotorcraft Forum, Cernobbio, Italy, 14 - 16 September 1993.

21. Van der Wall, B.G.: „CP-ROT First Results from Pressure Instrumented BO 105 Hingeless Model Rotor Tests", Paper No. C 22, Proceedings, 19th European Rotorcraft Forum, Cernobbio, Italy, September 1993.

22. Mercker, E., Pengel, K.: „Flow Visualization of Helicopter Blade Tip Vortices - A Quantitative Technique to Determine the Trajectory and Position of the Tip Vortex Pattern of a Model Rotor -", Paper No. 26, Proceedings, 18th European Rotorcraft Forum, Avignon, September 1992.

23. Lowson, M.V., Fiddes, S.P., Kloeppel, V., De Bernardis, E., Ianniello, S., Difrancescantonio, P.: „Theoretical Studies Undertaken During the HELINOISE Programme", Paper No. B 4, Proceedings, 19th European Rotorcraft Forum, Cernobbio, Italy, September 1993.